Forced pitch motion of wind turbines

2016 J. Phys.: Conf. Ser. 753 022042

(http://iopscience.iop.org/1742-6596/753/2/022042)

Forced pitch motion of wind turbines

V Leble[1] and G Barakos[2]

[1] Ph.D. Student, School of Engineering, University of Glasgow, Glasgow, UK
[2] Professor, School of Engineering, University of Glasgow, Glasgow, UK

E-mail: George.Barakos@glasgow.ac.uk

Abstract. The possibility of a wind turbine entering vortex ring state during pitching oscillations is explored in this paper. The aerodynamic performance of the rotor was computed using the Helicopter Multi-Block flow solver. This code solves the Navier-Stokes equations in integral form using the arbitrary Lagrangian-Eulerian formulation for time-dependent domains with moving boundaries. A 10-MW wind turbine was put to perform yawing and pitching oscillations suggesting the partial vortex ring state during pitching motion. The results also show the strong effect of the frequency and amplitude of oscillations on the wind turbine performance.

Nomenclature

Latin

A	Amplitude $[deg]$	t	Time $[s]$
M	Mach number [-]	U	Velocity $[m/s]$
L	Vertical temperature gradient $[K/m]$	v_i	Induced velocity $[m/s]$
Re	Reynolds number [-]	V_c	Inflow velocity $[m/s]$
T	Period $[s]$		

Greek

α	Angle $[deg]$	λ	Tip speed ratio [-]
β	Wind profile power coefficient [-]		

Abbreviations

BEM	Blade Element Momentum method	RWT	Reference Wind Turbine
CFD	Computational Fluid Dynamics	SST	Shear Stress Transport turbulence model
FOWT	Floating Off-shore Wind Turbine	URANS	Unsteady Reynolds-Averaged Navier-Stokes method
FVM	Free Vortex method	VLM	Vortex Lattice method
GDW	Generalised Dynamic Wake model	VRS	Vortex Ring State
rpm	Revolutions per minute		

1. Introduction

According to the European Wind Energy Association (EWEA), at the end of 2012, the total, installed offshore wind power was 5GW. During the first half of 2015, the European grid connected 584 commercial offshore wind turbines with a combined capacity of 2.3GW [1, 2].

Estimates for the year 2030 predict up to 11.3% coverage of total European electricity demand by offshore wind[3]. Similar trends are seen in the US, where onshore and offshore wind energy can provide up to 20% of the US electricity by 2030[4].

Projects under construction and planning confirm that the average water depths and distances to shore are likely to increase[5]. Shallow water regions suitable for constructing bottom-fixed, offshore wind turbines are limited. For depths exceeding 30-60 m, floating structures are economically more feasible. Hence, emphasis is placed on the development of floating offshore wind turbines (FOWTs). Unlike onshore machines, the FOWTs are highly dynamic since they are simultaneously subjected to the wind and wave loads and only constrained by mooring cables. Depending on the roughness of the sea, the FOWT may operate in various aerodynamic flow states, including windmill, propeller and transient states too. Figure 1 shows the hypothetical flow states of FOWT during pitching motion. Normally, a wind turbine will operate in the windmill state, extracting energy from the flow field. Excessive pitching motion of the FOWT may lead to a rapid change of the effective wind speed and tip speed ratio. In extreme cases, the rotor may also behave like a propeller. This potential cycling between the windmill and propeller states during pitching motion, and the intermediate flow conditions, poses operational and modelling challenges for FOWTs. The study of Sebastian and Lackner [6] indicated that the vortex ring state (VRS) occurrence is almost twice as likely for the floating systems, than for bottom-fixed turbines.

The pitching motion of the FOWT can also be enhanced by negative damping introduced by the conventional blade pitch controllers. Hydrodynamic damping will eventually limit the platform pitch amplitude, as was shown in [7], but higher amplitudes of motion will be experienced. In addition to the pitching motion, FOWTs are more likely than on-shore turbines to operate in yaw.

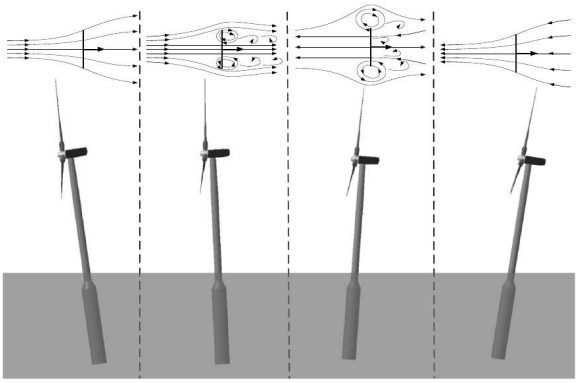

Figure 1. Hypothetical flow states of FOWT during pitching motion. From left to right: windmill state, turbulent wake state, vortex ring state and propeller state. Adapted from [8].

Clearly, the FOWT may experience complex aerodynamic flow states, and this has recently attracted research interest. A common approach is to employ simplified engineering models that assume incompressible potential flow. The Blade Element Momentum (BEM) method was used by Hansen and Cui[9] and by Madsen *et al.* [10] for yawed wind turbines. The Free-Vortex Method (FVM) combined with the BEM theory was used by Jeong *et al.*[11] to study the aero-elastic performance of 5MW wind turbines in yawed flow. The same technique was used by Xu *et al.*[12] for the fixed yaw case of Tjæreborg wind turbine [13]. A similar method was adopted by Qiu *et al.*[14], namely the Improved Free-Vortex Method (IFVM) combined with the nonlinear lifting line method for the blade aerodynamics. This method was applied to the wind turbines with fixed and dynamic yaw misalignments. The Vortex Lattice Method (VLM) was applied by Jeon *et al.*[15] to study a pitching wind turbine of rated power of 5MW, and with a variable speed controller. The work of de Vaal *et al.*[16] compared the results obtained with

unsteady BEM method and an actuator disc CFD approach for 5MW wind turbine undergoing surge motion. It was concluded that the BEM method agreed well with the actuator disc model, with differences when the wind turbine was enetring the turbulent wake state for part of the surging cycle. It was also suggested in this work to study yawing and pitching motions, since this can lead to improvements of BEM based methods. Sant and Cuschieri [17] made a comparison of BEM, Generalised Dynamic Wake (GDW) and FVM aerodynamic models. For the fixed yaw configurations of 5MW machine, the BEM model predicted considerably different changes in power and thrust as compared to other two models. The difference was contributed to the limitation of the BEM method.

The assumptions of those simplified models do not always hold for the complex aerodynamic flow states that can be encountered by FOWTs. For instance the assumptions of BEM and GDW models are violated when the wind turbine undergoes large pitching motion[6, 18]. Therefore, very recent works employed Navier-Stokes CFD solvers to study pitching wind turbines[8, 18]. Considerable differences were reported between predictions of BEM, GDW and URANS CFD methods. The papers relevant to the yaw and pitch conditions of the wind turbines are presented in Table 1.

Table 1. Some of the papers relevant for the analysis of yawing and pitching wind turbines.

Authors (Year)	Configuration	Structure	Numerical methods
Hansen and Cui[9] (1989)	Fixed/Dynamic Yaw	Rigid	BEM
Madsen *et al.*[10] (2003)	Fixed Yaw	Rigid/Elastic	BEM,URANS
Jeong *et al.*[11] (2013)	Fixed Yaw	Elastic	FVM
Qiu *et al.*[14] (2014)	Fixed/Dynamic Yaw	Rigid	IFVM
Jeon *et al.*[15] (2014)	Dynamic Pitch	Rigid	VLM
Tran and Kim[8, 18] (2015)	Dynamic Pitch	Rigid	BEM,GDW,URANS

In view of the above, the purpose of this paper is to present results of numerical computations for a 10-MW wind turbine undergoing prescribed pitching and yawing motions. The aerodynamic loads are computed using the Helicopter Multi-Block (HMB3) flow solver of Glasgow University[19]. The comparison to the aligned and fixed yaw cases is performed, and conclusions are drawn.

2. Test cases

The HMB3 flow solver of Glasgow University[19] and the DTU 10MW reference wind turbine (RWT) designed by Bak *et al.*[20] were employed in this paper. The wind turbine blade uses the FFA-W3 aerofoil family [21] with relative thickness ranging from 24% to 60%. The blade has non-linear distribution of the chord, relative thickness and twist. The rotor diameter is $178.3m$, and the wind turbine operates at a wind speed of $11m/s$ with a rotational speed of $8.8rpm$, resulting in the tip speed ration $\lambda = 7.5$. The blades have a pre-coning of 2.5° and nonlinear pre-bending with $3.3m$ displacement at the blade tip.

The test cases considered in this work are the wind turbine with constant yaw misalignment, and with sinusoidal yawing and pitching motions. The inflow was considered uniform for those cases, and the blades were assumed rigid. The list of all test cases is shown in Table 2.

2.1. Grid and computational parameters

The DTU 10MW RWT rotor was modelled including the nacelle, but without the tower. The grid consisted of $16.1M$ cells, giving $5.4M$ cells per blade. The normal distance for the first

Table 2. Description of presented test cases.

Name	Wind Turbine	Configuration	Angle/Amplitude	Period	Inflow	Blades
Y0	DTU	Aligned	$0°$	-	Uniform	Rigid
Y1	DTU	Fixed Yaw	$-3°$	-	Uniform	Rigid
Y2	DTU	Fixed Yaw	$3°$	-	Uniform	Rigid
Y3	DTU	Sinusoidal Yaw	$3°$	$8.8s$	Uniform	Rigid
P1	DTU	Sinusoidal Pitch	$3°$	$8.8s$	Uniform	Rigid
P2	DTU	Sinusoidal Pitch	$5°$	$8.8s$	Uniform	Rigid

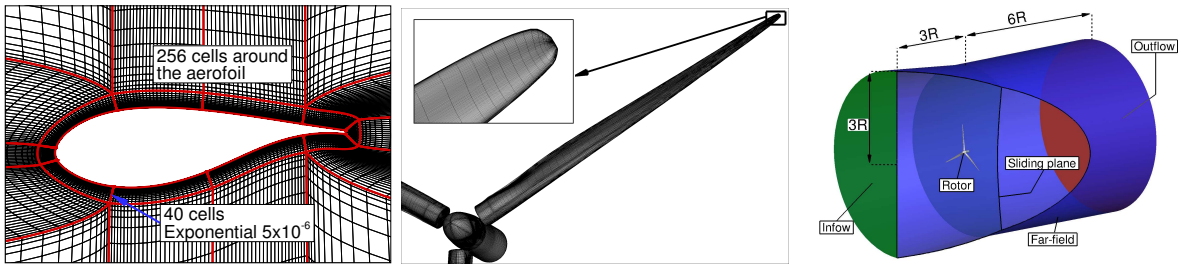

(a) Slice through the volume close to the blade surface.

(b) Surface mesh.

(c) Computational domain.

Figure 2. Grid employed for the DTU 10MW RWT rotor without the tower - (a) slice through the volume, (b) surface mesh, (c) computational domain for most of the cases, and (d) computational domain for case A2.

cells of the blocks adjacent to the blade surface was $5 \cdot 10^{-6}c$, where c is a maximum chord of the blade, $6.205m$. Based on the free-stream condition and the size of the first cell, the y^+ parameter was $y^+ = 0.9$. The first layer consisted of 40 cells in the normal direction to the blade surface, and 256 cells were distributed around the aerofoil section. The blade surface was resolved with 121 cells along the span. The domain consisted of the rotor that was attached to the nacelle through a sliding mesh plane [22]. An inflow boundary condition was placed three blade radii upstream of the rotor, and outflow was placed six blade radii downstream. The far-field was assigned three blade radii from the centre of rotation. The computational domain with the corresponding boundaries, a slice through the mesh close to the blade surface, and the surface mesh of the blade are shown in Figure 2.

The free-stream was kept to the level of turbulence of 2.6%, and the $k-\omega$ SST [23] turbulence model was employed. The time step for the unsteady computations was set to $\Delta t = 1.8 \cdot 10^{-2}s$, and corresponds to the time required for rotor to perform one degree of revolution. This step is thought to be adequate for the studied wind turbine. Work of Tran and Kim [8] employed 2.0 degree increment of azimuth angle.

3. Results and discussion

3.1. Static and dynamic yawing of DTU 10MW reference wind turbine

This section presents the results obtained for DTU 10MW reference wind turbine with static and dynamic yaw misalignments. First, the comparison of the aligned and static yaw cases is performed in this section. This involves comparison of the aligned case Y0 and fixed yaw case of $3°$ (Y2 in Table 2). Next, the sinusoidal yawing case Y3 with yaw amplitude $A = 3°$ and period $T_{yaw} = 8.8s$ is compared to the fixed yaw cases Y1 and Y2. The frequency of motion was chosen based on the most probable frequency of the sea waves for the wind speed of $11m/s$ [24].

The employed notation for yaw angles is shown in Figure 3(a). Positive yaw angle corresponds

to a reduced inflow angle for the blade at 12 o'clock or 0° of azimuth. Contrary, the blade at 180° of azimuth has increased inflow angle for positive yaw.

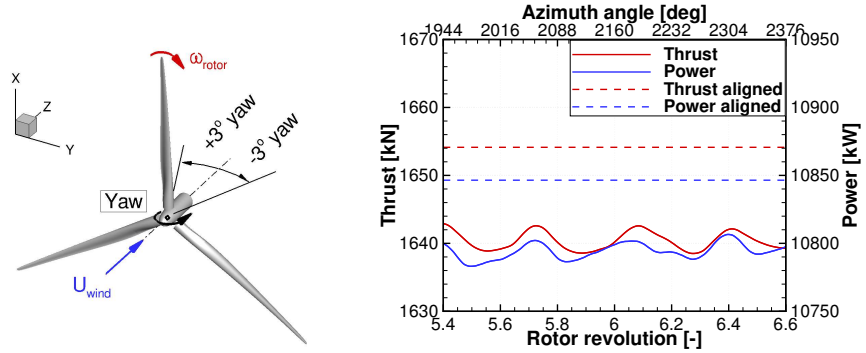

(a) Employed notation for yaw angle.

(b) Thrust and power.

Figure 3. Fixed yaw test cases: (a) employed notation for yaw angles, and (b) thrust and power as function of the rotor revolution.

The results for the fixed yaw case are shown in Figure 3(b). The periodic variation of thrust and power with the blade passing frequency is evident, and is caused by the advancing and retreating blade effect [25]. To be more specific, the blade is advancing in the upper half plane and retreating in the lower half plane with respect to the in-plane wind component. The results suggest average reduction of thrust by 0.8% and power by 0.5% due to the yaw misalignment. This agrees with observation of Krodstat and Adaramola[26] that the loss in power output is small (less than 3%) when the yaw angle is less than 10°.

Next, the DTU 10-MW RWT was forced to a yawing motion about a mean angle of 0°. The yaw amplitude was set to $A = 3°$, and the period of oscillation was $T_{yaw} = 8.8s$. The results in terms of power are shown in Figure 4. A periodic variation of power with the frequency of

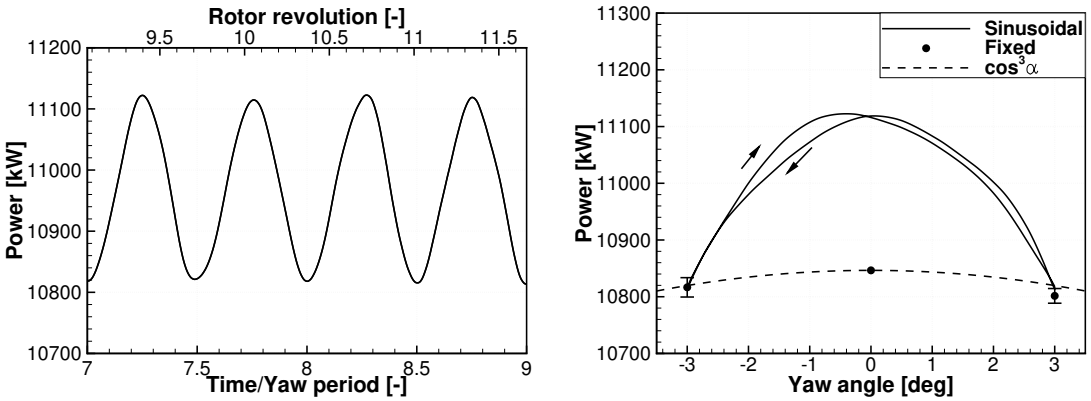

(a) Power as function of time.

(b) Power as function of yaw angle.

Figure 4. Power as function of time (a) and yawing amplitude (b).

yawing is visible. In this case, the frequency of rotation does not coincide with the frequency of yawing motion. This results in the asymmetries observed in Figure 4 due to the advancing and retreating blade effect [25]. Further, the power obtained for the fixed yaw cases is presented in

Figure 4(b) for comparison. The power variation with the yaw angle α may be approximated by $P(0°)\cos^x(\alpha)$, given that the yaw angle is fixed for each point [27]. The exponent x is often thought to be equal to 3. Experimental evidences suggest that the exponent x may vary between 1.8 and 5 [25]. Recent wind tunnel measurements shown that the curve based on $x = 3$ follows well measured data [26]. In this case, the exponent $x = 3$ shows good agreement with the computed power loss for fixed yaw misalignments, as can be seen in Figure 4(b). Error bars indicate the minimum and maximum value over the revolution.

The power production agrees between static and dynamic yaw cases for the maximum yaw angles. This is expected result, since the rotor has zero yawing velocity at maximum angle. However, the power variation due to the dynamic yaw motion shows larger amplitude, with the maximum value in the middle of the cycle. The increase in power production is about 2.5%, as compared to the aligned rotor case.

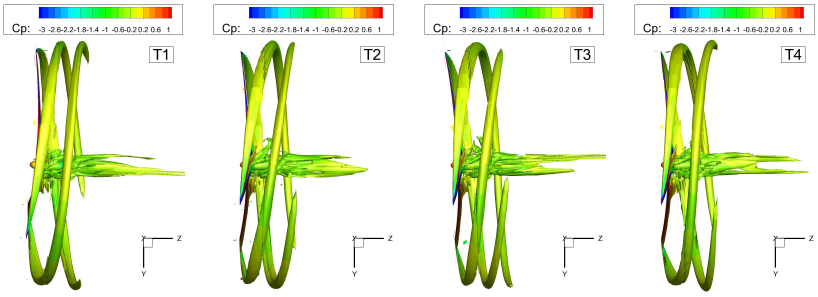

(a) Yaw $-3°$. (b) Yaw $0°$. (c) Yaw $3°$. (d) Yaw $0°$.

Figure 5. Instantaneous vortices visualised with the iso-surfaces of $Q = 0.05$ criterion coloured by the pressure coefficient C_P. Yawing amplitude $3°$, and yawing period $8.8s$.

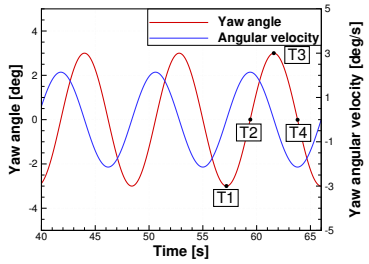

Figure 6. Yaw angle and yaw angular velocity as function of time.

Finally, Figure 5 shows the wake of the wind turbine at various instances visualised with the iso-surfaces of $Q = 0.05$ criterion. The presented instances correspond to the times shown in Figure 6, where the positive and negative yaw angles are defined in Figure 3(a).

3.2. Dynamic pitching of DTU 10MW reference wind turbine

The DTU 10MW RWT was forced to perform a sinusoidal pitching motion about the point located $119m$ below the rotor, and corresponds to the hub height in Bak *et al.*[20] The pitching amplitude was set to $A = 3°$ for the first test case (Test case P1), and to $A = 5°$ for the second test case (Test case P2). The mean pitch angle was zero degrees, and the period of motion for both cases was set to $T_{pitch} = 8.8s$. The frequency of the pitching motion was chosen based on the most probable frequency of the waves for the wind speed of $11m/s$ [24]. The results in terms

of thrust and power for both cases are compared in Figure 7. The results show large variations of the thrust and power. This agrees with the results presented in [18], where 5MW wind turbine undergoing pitching motion experienced from 0MW to 15MW of instantaneous aerodynamic power. Interestingly, the average thrust for both cases is close to the value obtained without the pitching *i.e.* about $1650kN$ of thrust. However, the mean power is about $12.3MW$ and $14.4MW$ for the pitching amplitudes of 3° and 5°, respectively. This corresponds to an increase of power by 13.4% and 32.8%, as compared to the power output of an aligned rotor not undergoing pitching motion.

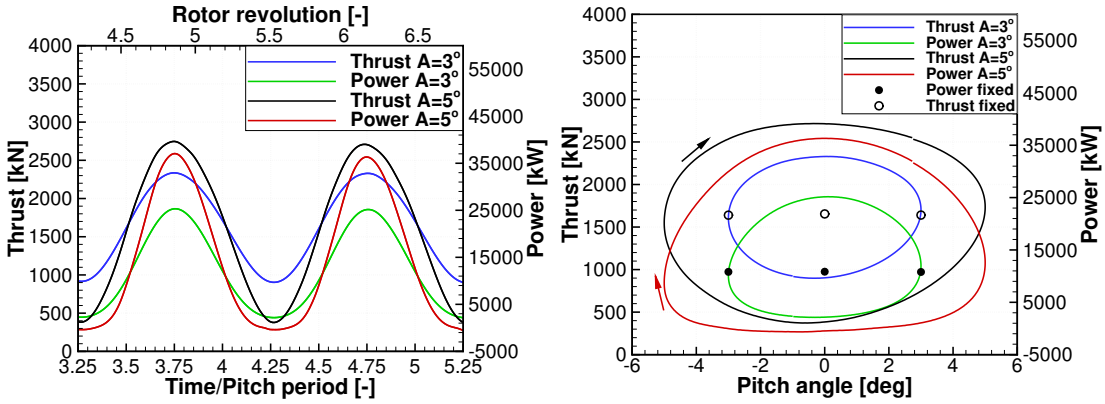

(a) Thrust and power as function of time (b) Thrust and power as function of pitch angle

Figure 7. Thrust and power as function of time (a) and pitching amplitude (b).

Figure 7(b) shows the thrust and power as functions of the pitch angle, where a hysteresis loop is observed. Figure 8 shows the wake of the wind turbine at various instances visualised with iso-surfaces of $Q = 0.05$ criterion. The presented instances correspond to the times shown in Figure 9, where negative pitch angle represents a wind turbine pitching towards the direction of the wind, while positive pitch angle represents the wind turbine pitching away of the wind.

Estimates of the induced velocity v_i were used to show that the wind turbine entered the turbulent wake or the vortex ring states. The induced velocity was estimated from the momentum theory in the applicable range, and the formula of Rand[28] was used otherwise, leading to the following expression for the rate of induced velocity

$$v_i/v_h = \begin{cases} -\frac{V_c}{2v_h} - \sqrt{(\frac{V_c}{2v_h})^2 - v_h^2} & \text{for } V_c/v_h \leq -2 \\ 1 - \frac{V_c}{2v_h} + \frac{25V_c^2}{12v_h^2} + \frac{7V_c^3}{6v_h^3} & \text{for } -2 < V_c/v_h < 0 \end{cases}, \tag{1}$$

where v_i is the induced velocity, $v_h = \sqrt{T/2\rho S}$ is the induced velocity in "hover" for the given thrust T and the rotor area S, and V_c is the inflow velocity normal to the rotor plane. The inflow velocity was computed from the wind speed U_{wind}, the linear velocity of the hub in the direction of the wind U_{hub}, and the pitch angle α as:

$$V_c = -(U_{wind}\cos(\alpha) + U_{hub}/\cos(\alpha)), \tag{2}$$

where the negative sign of inflow velocity was introduced to agree with the notation used for helicopters[28, 29]. The results are presented in Figure 10. As can be seen, the wind turbine did not encounter a vortex ring state for 3° of amplitude. This agrees with the fluctuations of thrust and power, where variations were almost symmetric with respect to the pitch angle. However, for the second test case ($A = 5°$) the rotor partially entered vortex ring state. The

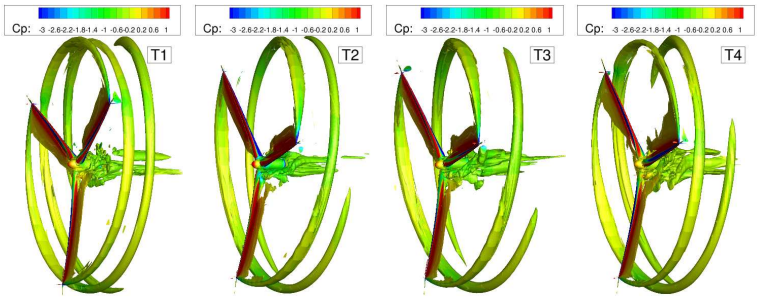

(a) Pitch $-3°$ (b) Pitch $0°$ (c) Pitch $3°$ (d) Pitch $0°$

(e) Pitch $-5°$ (f) Pitch $0°$ (g) Pitch $5°$ (h) Pitch $0°$

Figure 8. Instantaneous vortices visualised with the iso-surfaces of $Q = 0.05$ criterion coloured by the pressure coefficient C_P. Pitching period $8.8s$, pitching amplitude $3°$ (a-d), and $5°$ (e-h).

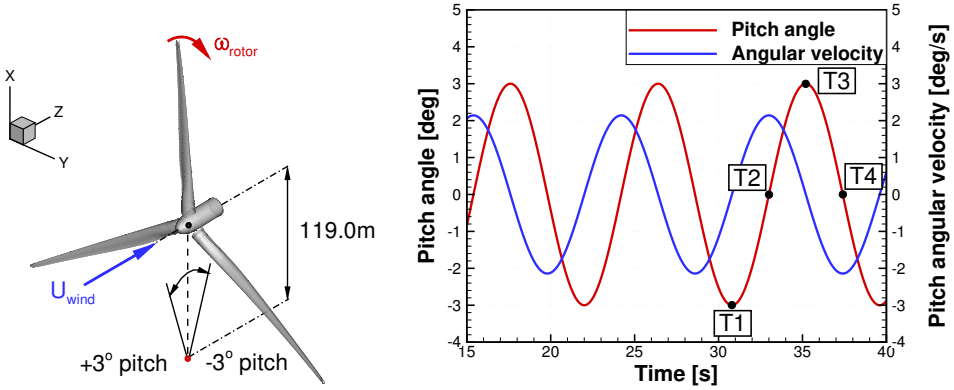

(a) Employed notation for pitch angles (b) Pitch angle and pitch velocity

Figure 9. Sinusoidal pitch test cases. Definition of the employed notation for pitch angles (a), and (b) the pitch angle and pitch angular velocity as function of time for pitching amplitude $3°$.

interaction between the blade and tip vortex can be seen in Figure 8(h) and 8(e). A closer look at Figure 7(a) shows the asymmetry of the thrust and power for pitch angle of $5°$ near maximum thrust and minimum power as the pitch velocity changes sign. The comparison of polars in Figure 7(b) revealed that the overall shape of the thrust and power with respect to the pitch angle was similar for both cases. The thrust force had a similar expansion towards lower and higher values as the amplitude of motion was increased, therefore maintaining almost the same averaged value (averaged over the cycle). However, the power curves showed a similar low-power part, where the difference in power for both cases was much smaller as compared to

the high-power part of the cycle. Although low power output was maintained for a longer part of the pitching cycle, as compared to the high-power part, the power averaged over the cycle increased as the amplitude of motion increased. Finally, the power showed a sharper increase as the turbine transitioned from backward to forward pitching motion. This can be seen in Figure 7(b).

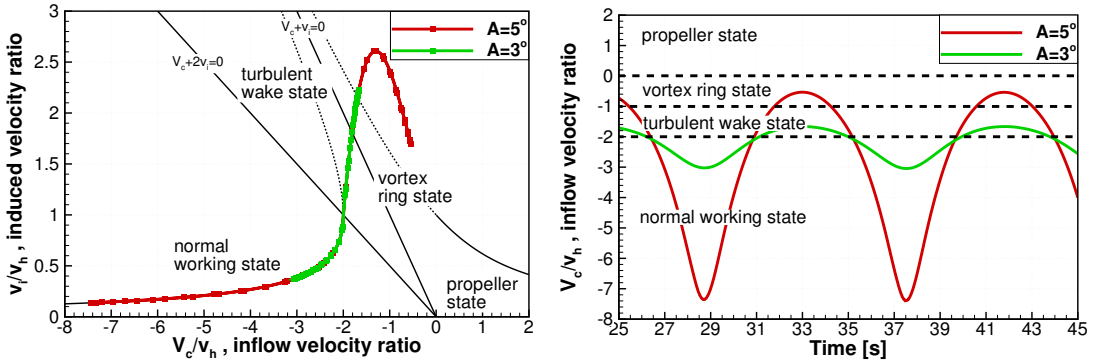

(a) Ratio of induced velocity (b) Ratio of inflow velocity

Figure 10. Estimated ratio of induced velocity as function of inflow velocity ratio (a), and ratio of inflow velocity as function of time (b) for pitching wind turbines with pitching amplitude of 3° and 5°.

4. Conclusions and future work

The paper presented the results of numerical computations for a 10-MW wind turbine undergoing prescribed motion in yaw and pitch. The HMB3 CFD solver was used to compute the aerodynamic flow and resulting loads on the wind turbine. The blades were considered rigid for the cases with prescribed motion, and the tower of the wind turbine was not included in the computational domain. The results showed large variations in thrust and power as the wind turbine pitched about a point located $119m$ below the rotor. The vortex ring state was encountered when the wind turbine was forced to a pitching motion with amplitude of 5° and period of $8.8s$. The results suggest larger variations in power for the case of dynamic yaw, as compared to fixed yaw cases. Differences of up to 2.5% were seen for the studied dynamic yaw cases. However, the largest changes of thrust and power were obtained for the pitching motion of the rotor. Differences of up to 32.8% were seen for the cases studied.

Acknowledgments

The financial support of the Marie Curie Host Fellowships Program: FP7-PEOPLE-2012-ITN--309395 - New Materials And Reliability In Offshore Wind Turbines Technology "MARE-WINT" is gratefully acknowledged (`http://www.marewint.eu/`). Results were obtained using the EPSRC funded ARCHIE-WeSt High Performance Computer (`www.archie-west.ac.uk`). EPSRC grant no. EP/K000586/1.

References

[1] Corbetta G and Mbistrova A 2015 The European offshore wind industry - key trends and statistics 2014 Report European Wind Energy Association, EWEA
[2] Ho A and Mbistrova A 2015 The European offshore wind industry - key trends and statistics 1st half 2015 Report European Wind Energy Association, EWEA

[3] Corbetta G, Ho A, Pineda I, Ruby K, Van de Velde L and Bickley J 2015 Wind energy scenarios for 2030 Report European Wind Energy Association, EWEA
[4] Fried L, Qiao L, Sawyer S, Shukla S and Bitter L 2014 Global wind report 2014: Annual market update Online Global Wind Energy Council, GWEC
[5] Arapogianni A, Genachte A B, Ochagavia R M, Vergara J P, Castell D, Tsouroukdissian A R, Korbijn J, Bolleman N C, Huera-Huarte F J, Schuon F, Ugarte A, Sandberg J, de Laleu V, Maciel J, Tunbjer A, Roth R, de la Gueriviere P, Coulombeau P, Jedrec S, Philippe C, Voutsinas S, Weinstein A, Vita L, Byklum E, Hurley W L and Grubel H 2013 Deep water - The next step for offshore wind energy Report European Wind Energy Association, EWEA
[6] Sebastian T and Lackner M A 2011 *Proceedings of 49th AIAA Aerospace Sciences Meeting* (Orlando, Florida)
[7] Koyanagi T, Karikomi K, Iwasaki S and Nakamura A 2015 *Proceedings of DEWEK 2015 conference* (Bremen, Germany)
[8] Tran T T and Kim D H 2015 *Journal of Wind Engineering and Industrial Aerodynamics* **142** 65–81 ISSN 0167-6105 URL http://dx.doi.org/10.1016/j.jweia.2015.03.009
[9] Hansen A C and Cui X 1989 *Journal of Solar Energy Engineering* **111** 367–371 ISSN 0199-6231 URL http://dx.doi.org/10.1115/1.3268336
[10] Madsen H A, Sorensen N N and Schreck S 2003 *ASME 2003 Wind Energy Symposium* (ASME) pp 94–103 ISBN 1-56347-594-4 URL http://dx.doi.org/10.1115/wind2003-519
[11] Jeong M S, Kim S W, Lee I, Yoo S J and Park K 2013 *Renewable Energy* **60** 256–268 ISSN 0960-1481 URL http://dx.doi.org/10.1016/j.renene.2013.05.014
[12] Xu B F, Wang T G, Yuan Y and Cao J F 2015 *Philosophical Transactions of the Royal Society of London A: Mathematical, Physical and Engineering Sciences* **373** ISSN 1364-503X URL http://dx.doi.org/10.1098/rsta.2014.0080
[13] Snel H and Schepers J 1995 Joint investigation of dynamic inow effects and implementation of an engineering method Technical Report ECN-C-94107 Energy research Center of the Netherlands, ECN
[14] Qiu Y X, Wang X D, Kang S, Zhao M and Liang J Y 2014 *Renewable Energy* **70** 93 – 106 ISSN 0960-1481 URL http://dx.doi.org/10.1016/j.renene.2014.03.071
[15] Jeon M, Lee S and Lee S 2014 *Renewable Energy* **65** 207 – 212 ISSN 0960-1481 URL http://dx.doi.org/10.1016/j.renene.2013.09.009
[16] de Vaal J, Hansen M and Moan T 2014 *Wind Energy* **17** 105–121 ISSN 1099-1824 URL http://dx.doi.org/10.1002/we.1562
[17] Sant T and Cuschieri K 2016 *Journal of Solar Energy Engineering* **138** 031004–031004 ISSN 0199-6231 URL http://dx.doi.org/10.1115/1.4032684
[18] Tran T and Kim D 2015 *Journal of Mechanical Science and Technology* **29** 549–561 ISSN 1738-494X URL http://dx.doi.org/10.1007/s12206-015-0115-0
[19] Brocklehurst A, Steijl R and Barakos G 2008 *34th European Rotorcraft Forum* (ERF)
[20] Bak C, Zhale F, Bitsche R, Kim T, Yde A, Henriksen L C, Andersen P B, Natarajan A and MH H 2013 Description of the dtu 10 mw reference wind turbin Technical Report I-0092 DTU Wind Energy
[21] Björck A Coordinates and caluclations for the FFA-W1-xxx, FFA-W2-xxx and FFA-W3-xxx series of airfoils for horizontal axis wind turbines Technical Report FFA TN 1990-15 The Aeronautical Research Institute of Sweden, FFA
[22] Steijl R and Barakos G 2008 *International Journal for Numerical Methods in Fluids* **58** 527–549 ISSN 1097-0363 URL http://dx.doi.org/10.1002/fld.1757
[23] Menter F 1994 *AIAA Journal* **32** 1598–1605 ISSN 0001-1452 URL http://dx.doi.org/10.2514/3.12149
[24] Lee W T, Bales S L and Sowby S E 1985 *Standardized Wind and Wave Environments for North Pacific Ocean Areas* (David W. Taylor Naval Ship Research and Development Center)
[25] Schepers J G 2012 *Engineering models in wind energy aerodynamics: Development, implementation and analysis using dedicated aerodynamic measurements* Ph.D. thesis Wind Energy Department Delft University of Technology
[26] Krogstad P Å and Adaramola M S 2012 *Wind Energy* **15** 743–756 ISSN 1099-1824 URL http://dx.doi.org/10.1002/we.502
[27] Burton T, Sharpe D, Jenkins N and Bossanyi E 2002 *Wind Energy Handbook* (Chichester, UK: John Wiley & Sons, Ltd) ISBN 9780470846063
[28] Rand O 2006 *Journal of the American Helicopter Society* **51** 279–282
[29] Leishman J G 2006 *Principles of Helicopter Aerodynamics* 2nd ed (Cambridge University Press) ISBN 9780521858601